









Controlled modulation of the dynamics of the *Deinococcus grandis* Dps N-terminal tails by divalent metals

João P. L. Guerra^{1,2}  | Clement E. Blanchet³  | Bruno J. C. Vieira⁴  |
 João C. Waerenborgh⁴  | Nykola C. Jones⁵  | Søren Vrønning Hoffmann⁵  |
 Alice S. Pereira^{1,2}  | Pedro Tavares^{1,2} 

¹UCIBIO – Applied Molecular Biosciences Unit, Department of Chemistry, NOVA School of Science and Technology | FCT NOVA, Universidade NOVA de Lisboa, Caparica, Portugal

²Associate Laboratory i4HB – Institute for Health and Bioeconomy, NOVA School of Science and Technology | FCT NOVA, Universidade NOVA de Lisboa, Caparica, Portugal

³European Molecular Biology Laboratory, Hamburg Outstation, Hamburg, Germany

⁴Centro de Ciências e Tecnologias Nucleares, DECN, Instituto Superior Técnico, Universidade de Lisboa, Bobadela LRS, Portugal

⁵ISA, Department of Physics and Astronomy, Aarhus University, Aarhus, Denmark

Correspondence

Pedro Tavares and Alice S. Pereira,
 Department of Chemistry, NOVA School
 of Science and Technology | FCT NOVA,
 2829-516 Caparica, Portugal.
 Email: pabt@fct.unl.pt (P. T.) and
 Email: masp@fct.unl.pt (A. S. P.)

Funding information

Fundação Ciência e Tecnologia - MCTES,
 Grant/Award Numbers: COVID/
 BD/152497/2022, LA/P/0140/2020,
 LISBOA-01-0145-FEDER-022096,
 LTHMFL-NECL, PD/00193/2012, PD/
 BD/135476/2017, PTDC/BIA-
 PRO/111485/2009, PTDC/
 QUI/64248/2006, UID/Multi/04349/2019,
 UIDB/00068/2020, UIDB/04378/2020;
 Horizon 2020 Framework Programme,
 Grant/Award Number: 730872 -
 CALIPSOplus

Review Editor: Aitziber L. Cortajarena

Abstract

DNA-binding proteins from starved cells (Dps) are small multifunctional nanocages expressed by prokaryotes in acute oxidative stress conditions or during the starvation-induced stationary phase, as a bacterial defense mechanism. Dps proteins protect bacterial DNA from damage by either direct binding or by removing precursors of reactive oxygen species from solution. The DNA-binding properties of most Dps proteins studied so far are related to their unordered, flexible, N- and C-terminal extensions. In a previous work, we revealed that the N-terminal tails of *Deinococcus grandis* Dps shift from an extended to a compact conformation depending on the ionic strength of the buffer and detected a novel high-spin ferrous iron center in the proximal ends of those tails. In this work, we further explore the conformational dynamics of the protein by probing the effect of divalent metals binding to the tail by comparing the metal-binding properties of the wild-type protein with a binding site-impaired D34A variant using size exclusion chromatography, dynamic light scattering, synchrotron radiation circular dichroism, and small-angle X-ray scattering. The N-terminal ferrous species was also characterized by Mössbauer spectroscopy. The results herein presented reveal that the conformation of the N-terminal tails is altered upon metal binding in a gradual, reversible, and

SAXS Datasets Accession numbers SASDQT4, SASDQU4, SASDQV4, SASDQW4, SASDQX4, SASDQY4, SASDQZ4, SASDQ25, SASDQ35, SASDQ45, SASDQ55, SASDQ65, SASDQ75, available at the Small Angle Scattering Biological Data Bank (SASBDB).

This is an open access article under the terms of the [Creative Commons Attribution-NonCommercial-NoDerivs](https://creativecommons.org/licenses/by-nc-nd/4.0/) License, which permits use and distribution in any medium, provided the original work is properly cited, the use is non-commercial and no modifications or adaptations are made.

© 2023 The Authors. *Protein Science* published by Wiley Periodicals LLC on behalf of The Protein Society.

specific manner. These observations may point towards the existence of a regulatory process for the DNA-binding properties of Dps proteins through metal binding to their N- and/or C-terminal extensions.

KEYWORDS

biological small-angle X-ray scattering, conformational dynamics, DNA-binding protein from starved cells (Dps), metal binding, mini-ferritin, Mössbauer spectroscopy, N-terminal tail extensions

1 | INTRODUCTION

DNA-binding proteins from starved cells (Dps) protect bacteria from reactive oxygen species formed during acute oxidative or starvation stresses. They can shield the bacterial chromosome directly through DNA binding and condensation and/or indirectly by removing toxic Fe^{2+} ions and hydrogen peroxide from the intracellular medium, via ferroxidation and mineralization reactions (as members of the Ferritin family) (Guerra et al. 2021). The structure of Dps proteins resembles a 9–10 nm wide hollow 3D-squiracle shell, resulting from the self-assembly of 12 identical subunits, and contain 12 catalytic ferroxidase centers (FOCs) (Grant et al. 1998; Crichton and Declercq 2010). Each monomer is folded in a conserved four-helix bundle motif and presents N- and C-terminal tail extensions that vary considerably in amino acid composition and length (from 2 to ~50 residues long) (Guerra et al. 2021; Roy et al. 2007).

The structural properties of the tails remain elusive due to their disordered nature. While packed against the dodecamer shell in virtually all of the crystal structures published thus far, recent small-angle X-ray scattering (SAXS) data revealed that, in certain experimental conditions, the N-terminal tails extend outwards into a star-shaped conformation with increased solvent accessibility (Santos et al. 2017; Dubrovin et al. 2021). The current understanding of the DNA-binding properties of Dps proteins focus on the electrostatic interactions between positive residues in the N-terminal tails and the negative phosphate groups in the DNA (Ceci et al. 2004; Karas et al. 2015). In fact, the modification, truncation, or removal of the N-terminal tails impairs the DNA-binding properties of the protein (Roy et al. 2007; Bhattacharyya and Grove 2007; Jacinto et al. 2021). Dps homologues with shorter, neutral, and/or spatially inaccessible N- or C-terminal tails are generally unable to bind and compact DNA (Bozzi et al. 1997; Papinutto et al. 2002). The chemical composition of the solvent (namely pH, concentration of NaCl or Mg^{2+}) is a key factor in the regulation of the DNA binding process, that also affects the conformation of the N-terminal tails (Huergo et al. 2013; Lee et al. 2015; Dadinova et al. 2021; Soshinskaya et al. 2020).

Although iron is the primary substrate of Dps, the binding of other metals to Dps proteins is a relatively common topic explored in different areas, such as structural biochemistry, enzymology, and nanobiotechnology (Guerra et al. 2021). The interaction with different divalent metal ions has been described, most notably Zn^{2+} and Mn^{2+} , but also Cu^{2+} , Co^{2+} , Ni^{2+} , Cd^{2+} , and Mg^{2+} (Dadinova et al. 2021; Alaleona et al. 2010; Haikarainen et al. 2011; Kim et al. 2006; Nguyen and Grove 2012; Yokoyama et al. 2012; Cuypers et al. 2007). Interestingly, besides the ferroxidase binding sites (located at each dimer interface; 12 FOCs per protein molecule; Figure 1), the proximal end of the N-terminal tail of *Deinococcus* (*D.*) *radiodurans* Dps1 exhibits an additional metal-binding site, thus far crystallized with Zn^{2+} and Co^{2+} (Kim et al. 2006; Romão et al. 2006). The functional and structural impact of this metal-binding site is still relatively uncharacterized, but it is believed to be important for DNA binding (Bhattacharyya and Grove 2007; Nguyen and Grove 2012).

Our previous work revealed that the N-terminal tail of *Deinococcus grandis* Dps (DgrDps) can adopt a dynamic range of conformations modulated by the ionic strength and coordinates a novel iron-binding site within mini-ferritins (Guerra et al. 2022). Considering these results and the structural model of DgrDps (which shares 77% identity with homologous *D. radiodurans* Dps1 amino acid sequence), we hypothesized that the metal-binding site found in the proximal end of the N-terminal tails (conserved residues Asp34, His37, His48, and Glu53, DgrDps numbering, as represented in Figure 1) might bind the substrate ferrous iron. Thus, a single-residue mutation, DgrDps D34A (substitution of aspartate 34 by an alanine) was designed to impair this metal binding site. In this work, we confirm that Asp34 is an important ligand of the novel high-spin ferrous binding site previously described using Mössbauer spectroscopy and further explore the modulation of the conformational dynamics of the N-terminal tails by different relevant divalent metals such as Zn^{2+} , Co^{2+} , Mn^{2+} , and Mg^{2+} using size exclusion chromatography (SEC), dynamic light scattering (DLS), synchrotron radiation circular

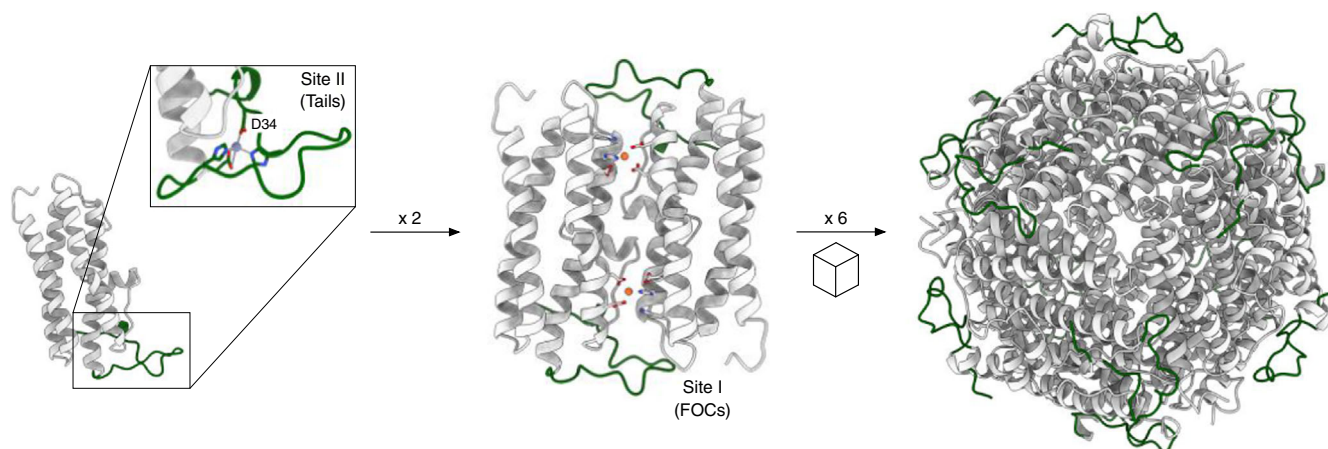


FIGURE 1 The iron binding sites in DgrDps. Left: Model of the DgrDps monomer with the four-helix bundle motif in gray and the N-terminal tail in green. Inset: Amplification of the residues that comprise the tail metal binding site shown as sticks, here termed Site II (Asp34, His37, His48, and Glu53), obtained via homology modeling (Waterhouse et al. 2018) using *D. radiodurans* Dps1 (PDB 2C2U) as template. Middle: The antisymmetric dimer, with the residues that comprise the ferroxidase centers shown as sticks (FOCs, designated as Site I): His81, His93, Asp97, Asp108, and Glu112. Two FOCs are formed per dimer interface. Right: The quaternary structure of DgrDps is achieved after self-assembly of six dimers into a spherical cube-shaped dodecamer, with a total of 12 FOCs and 12 N-terminal tail metal binding sites.

dichroism (SRCD), and small-angle X-ray scattering (SAXS).

2 | RESULTS

2.1 | Characterization of the DgrDps D34A protein variant

To confirm the dynamics of the N-terminal tails of the D34A variant, the effect of the ionic strength was assessed by SEC and DLS, as previously performed using the DgrDps WT and ΔN (with the first 46 amino acid residues truncated) proteins (Guerra et al. 2022). The results presented in Figure 2 show that the apparent molecular size of the D34A protein particle in solution is also dependent on the ionic strength of the buffer, with a similar range of apparent Stokes radii and hydrodynamic diameters. Table S1 comprises the data obtained. Similar to DgrDps WT, the elution volume of the D34A variant decreases from 12.1 ± 0.1 mL to 10.3 ± 0.1 mL as the NaCl concentration increases from 50 to 480 mM, corresponding to an apparent raise of the R_s from 4.9 ± 0.1 to 6.6 ± 0.1 nm. Likewise, the Z-Average of D34A increases from 12.6 ± 0.6 nm to 15.0 ± 0.4 , with all PI values below 0.2, indicating low polydispersity (Stetefeld et al. 2016). Based on the conclusions from our previous work (Guerra et al. 2022), this increase in the apparent size of the macromolecule is likely due to the dynamic shift of the N-terminal tails from the compact to the extended conformation. Moreover, the single mutation did not

affect the ferroxidation and iron mineralization activity of D34A. Taken together, these results indicate that the DgrDps D34A variant behaves like the WT protein at the structural and functional levels and that the N-terminal tails maintain their properties, aside from the putative loss of the metal-binding ability due to the disruption of the metal coordination sphere.

2.2 | Mössbauer spectroscopic characterization of the N-terminal tail iron-binding site

A novel iron-binding site in DgrDps was characterized in previous experiments and the origin of the high-spin ferrous Mössbauer species was attributed to the binding at the N-terminal tails site by comparison with a tailless variant of the protein (DgrDps ΔN). To further study the role of this metal-binding site, samples of the DgrDps D34A variant in the extended conformation (in 200 mM MOPS pH 7.0, 200 mM NaCl) were incubated with $^{57}\text{Fe}^{2+}$ ions in the absence of any oxidating co-substrate and analyzed using Mössbauer spectroscopy. Figure 3 shows the Mössbauer spectra of D34A samples reacted with different ratios of ferrous iron per dodecamer. As with DgrDps ΔN , the spectra are explained by the contributions of two quadrupole doublets typical of ferrous species. A single sharp doublet is detected at the lowest substoichiometry, 6 Fe/D34A protein (6 Fe/D34A protein represents the addition of 0.5 Fe^{2+} ions per monomer), with parameters characteristic of the FOC (Site I, with $\delta = 1.27$

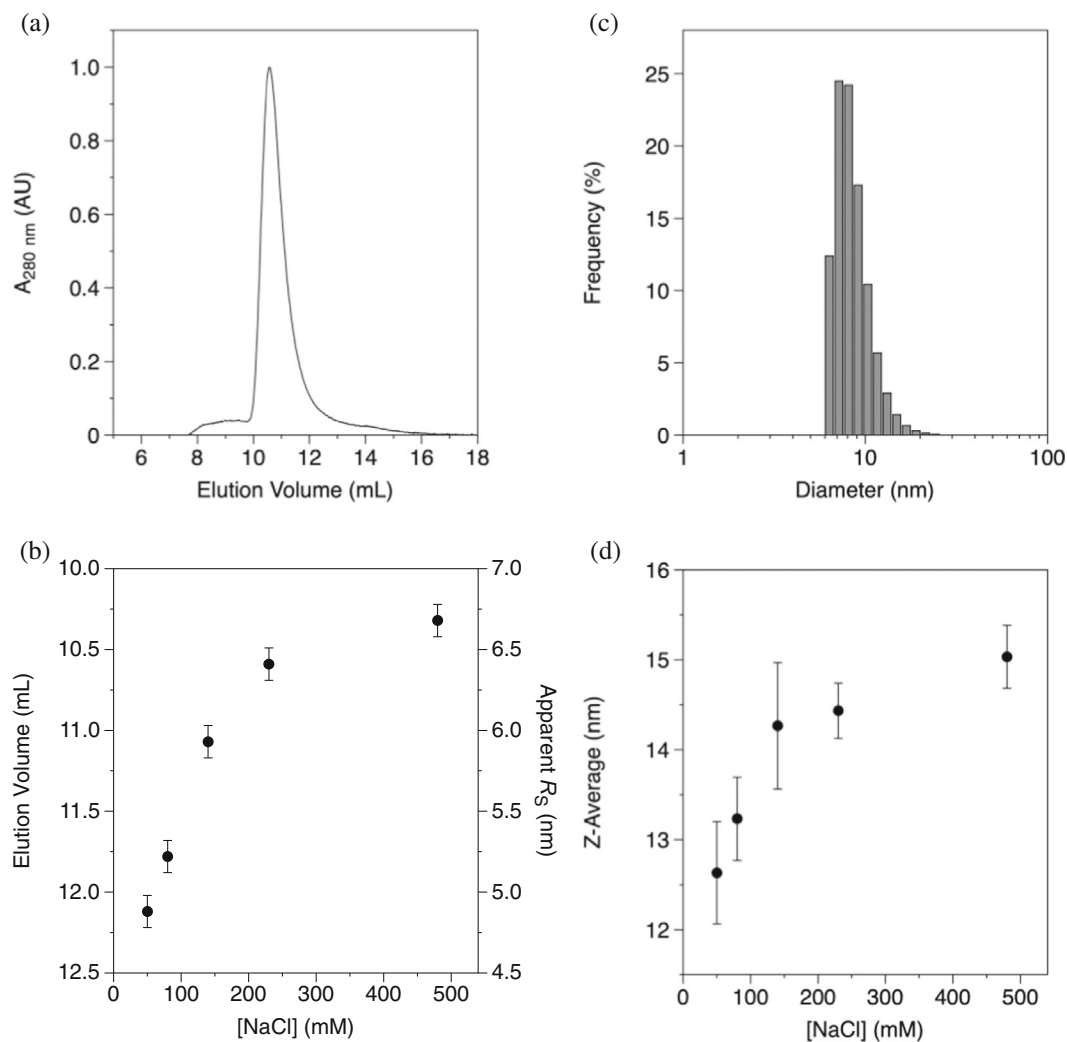


FIGURE 2 Macromolecular properties of the DgrDps D34A variant. (a) Elution profile on a calibrated Superdex 200 10/300 SEC column in 200 mM MOPS pH 7.0, 200 mM NaCl; (b) Dependence of the SEC elution volumes and estimated Stokes radii with the ionic strength (in 50 mM MOPS pH 7.0 and varying NaCl concentrations, from 50 to 480 mM); (c) Particle size distribution by DLS, in 200 mM MOPS pH 7.0, 200 mM NaCl; and (d) DLS hydrodynamic diameter (Z-Average) as a function of the ionic strength of the sample buffer, as described in (b).

± 0.01 mm/s and $\Delta E_Q = 2.83 \pm 0.02$ mm/s). Incubation with higher amounts of ferrous substrate results in the appearance of additional ferrous species ($\delta = 1.33 \pm 0.02$ mm/s, $\Delta E_Q = 3.22 \pm 0.03$ mm/s) due to the non-specific binding of Fe^{2+} ions in the protein channels or aqueous ferrous complexes (the latter most likely in a very small percentage due to the high affinity of the protein to the substrate). Notably, and similar to the tailless protein variant, the D34A spectra lack the peak at lower energies found in DgrDps WT, previously attributed to the N-terminal tail species (named Site II, with $\delta = 1.10 \pm 0.02$ mm/s and $\Delta E_Q = 3.82 \pm 0.02$ mm/s) (Guerra et al. 2022). As expected, Site I reaches a maximum occupancy at 11.3 ± 1 Fe/protein (Figure S1). Based on these observations, it is reasonable to conclude that Site II species, uniquely present in the WT, results from the

coordination of a ferrous ion by residues in the metal-binding site present at the proximal end of each of the 12 N-terminal tails, with the Asp34 residue being absolutely required to establish the first coordination sphere. Table 1 summarizes the Mössbauer parameters obtained by least squares fit analysis of the experimental data.

2.3 | Impact of metal binding on the dynamic conformation of the N-terminal tails

Several different physiologically relevant modulators of the structural and functional properties of the N-terminal tails may exist *in vivo*, such as pH, substrate (iron) levels, interaction with biomolecular partners (other proteins

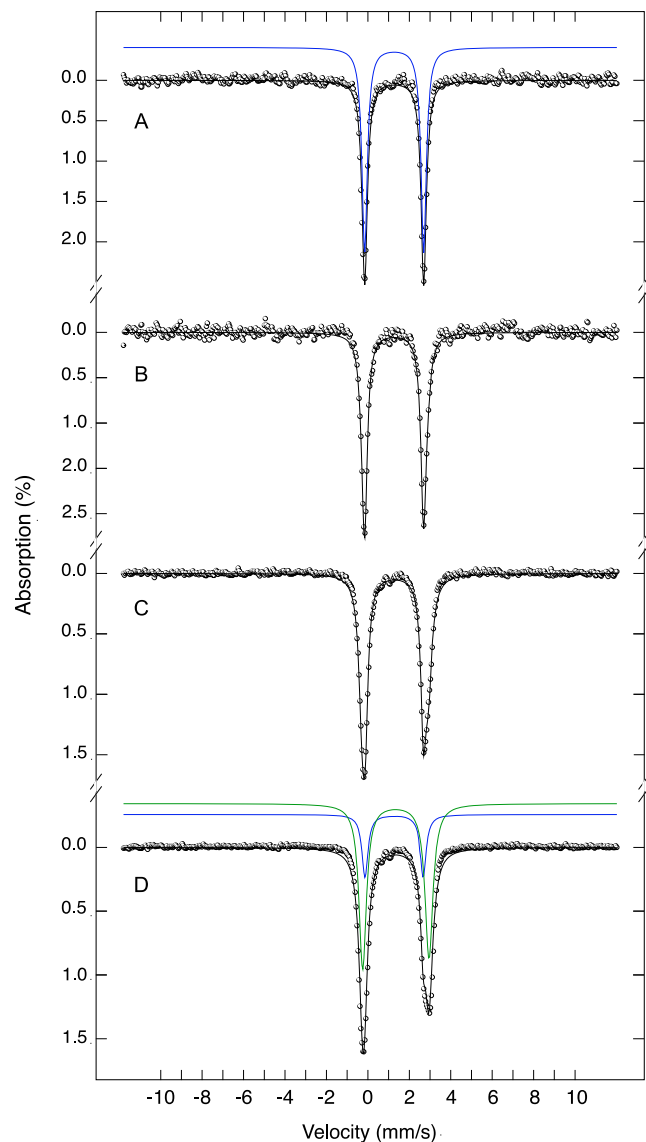


FIGURE 3 Mössbauer spectra of the anaerobic ferrous loading of DgrDps D34A. Apo-protein samples were incubated with different concentrations of $^{57}\text{Fe}^{2+}$ ions: $[\text{Fe}^{2+}]/[\text{Dps}]$ molar ratio of 6 (a), 12 (b), 24 (c), and 48 (d). The spectra were recorded at 80 K, with no external magnetic field applied. The solid lines overlaying the experimental spectra are the result of least squares fits to the data (relevant parameters listed in Table 1). The contribution of Site I and additional ferrous species are represented as blue and green lines, respectively.

and/or DNA), among others. As mentioned before, divalent metals (transition metals such as Zn^{2+} , Co^{2+} , and Mn^{2+} or alkaline earth metals such as Mg^{2+}) are well known to interact with Dps proteins. The recently established existence of a divalent metal-binding site in the proximal end of each N-terminal tail of DgrDps and its ability to bind ferrous ions, as revealed by Mössbauer spectroscopy, prompted the question: Can the occupation of the metal-binding site at the N-terminal tail affect its

conformation in a controlled and dynamic process, like the effect previously described for the ionic strength dependence? To try to answer, both DgrDps WT and D34A proteins were reacted with different divalent metals (Zn^{2+} , Co^{2+} , Cd^{2+} , Ni^{2+} , Mn^{2+} , Mg^{2+} , and Ca^{2+}), at high ionic strength (50 mM MOPS pH 7.0, 230 mM NaCl) to ensure a starting point with the stable, extended conformation.

The SEC elution profiles of the DgrDps WT samples incubated with 24 molar equivalents (24 $\text{M}^{2+}/\text{protein}$ oligomer) of each metal (Figure 4a and Table S2) reveal two sets of chromatographic peaks. Incubation of the protein with Ni^{2+} , Mn^{2+} , Ca^{2+} , and Mg^{2+} ions did not affect the elution volume (V_e) relatively to the apo-form (metal-free) of the protein, with $V_e = 10.7 \pm 0.1$ mL, whereas reaction with Zn^{2+} , Co^{2+} , and Cd^{2+} increased the elution volume to $\sim 11.5 \pm 0.1$ mL, which corresponds to a smaller apparent R_s (shifting from 6.1 ± 0.1 to 5.5 ± 0.1 nm), closer to the compact conformation behavior. In turn, superimposable elution profiles were obtained in a parallel experiment with the DgrDps D34A variant (Figure 4b), analogous to the apo-form of the protein (with a peak between 10.6 and 10.8 mL), characteristic of the extended conformation. Moreover, a gradual shift toward the peak with larger elution volume was observed when the protein was titrated with Zn^{2+} ions (with 6–48 $\text{Zn}^{2+}/\text{protein}$), as shown in Figure 4c (V_e shifted from 10.6 ± 0.1 mL for the apo-form to 11.6 ± 0.1 mL for the sample with 48 Zn^{2+} equivalents). Interestingly, this shift was almost totally reverted by the addition of an excess of EDTA to the sample loaded with 48 equivalents of Zn^{2+} (chromatographic peak at 10.9 ± 0.1 mL).

Likewise, DgrDps WT and D34A proteins were reacted with 12 and 24 molar equivalents of either Zn^{2+} , Co^{2+} , Cd^{2+} , Mn^{2+} , and Mg^{2+} and analyzed using DLS. The results are presented in Figure 4d and listed in Table S3. In general, the DLS results corroborate those obtained by SEC, with the addition of Zn^{2+} , Co^{2+} , and Cd^{2+} ions leading to a decrease in the hydrodynamic size of the DgrDps WT samples from 16.2 ± 0.5 nm to 13.3 ± 1.0 nm. On the contrary, addition of Mn^{2+} and Mg^{2+} ions did not alter the Z-Average value of the protein (~ 16 nm). Additionally, the hydrodynamic diameter of DgrDps D34A variant remained constant within the error of the technique (14.3 ± 0.8 nm) and consistent with the value determined for the apo-form, regardless of the amount and type of metal added. Once again, considering the three metals that affected the DgrDps WT apparent particle size, incubation with larger amounts of the metal progressively induced the conversion to a protein population with smaller Z-Average values. In terms of homogeneity and dispersity of each sample, the addition of the divalent metals did not affect the PI values, which

TABLE 1 Mössbauer parameters of iron species in DgrDps D34A variant

Parameters for ferrous species in iron loaded DgrDps D34A				
	Site I		Additional ferrous	
δ (mm/s)	1.27 (1)		1.33 (2)	
ΔE_Q (mm/s)	2.83 (2)		3.22 (3)	
Linewidth (mm/s)	0.32 (2)		0.41 (4)	
Iron ratio	%	Occupancy	%	Occupancy
6	100	6 (0)	0	0
12	88 (2)	11 (1)	12 (5)	1 (1)
24	47 (2)	11 (1)	53 (5)	13 (1)
48	24 (2)	11 (1)	76 (5)	37 (2)

Note: The contribution of the iron species in each spectrum is given in percentage and occupancy values. Values in brackets are uncertainties of the last significant digits.

remained between 0.1 and 0.3, throughout the experiment denoting highly monodisperse particles, with uniform size and shape.

The overall secondary structure of metal-loaded DgrDps WT and D34A proteins was analyzed using SRCD and compared with their apo-forms. Spectra were recorded after incubating the protein with different amounts of each divalent metal tested (0–24 M^{2+} per protein) at 25°C. The results are shown in Figure 5. The spectra exhibit a significant contribution of helical structures (with a maximum at 193 nm and minima at 208 and 222 nm) in every condition tested, suggesting that the binding of the divalent metal does not significantly alter the secondary structure of the proteins. The experimental datasets were then analyzed using DichroWeb server for estimation of the content of each secondary structure element (Table S4). Using the reference dataset SP175 optimized for the 175–240 nm range and the analysis program CDSSTR, DichroWeb analysis revealed no significant variation of the content of secondary elements upon incubating the proteins with Zn^{2+} , Co^{2+} , Mn^{2+} , or Mg^{2+} , at any concentration, with the percentage values differing only within the error of the technique. Moreover, the results obtained for DgrDps D34A are similar to DgrDps WT regardless of the experimental conditions used.

Together, the results from the SEC, DLS, and SRCD analyses on the effect of divalent metal on the structure of DgrDps WT and D34A proteins suggest that the binding to the metal-binding site present in the N-terminal tail induces a conformational change of the tail without affecting the overall secondary structure of the protein, in a behavior apparently similar to the one described for the ionic strength dependence (Guerra et al. 2022). This effect is specific, and the occupancy of the binding site is concentration dependent, since only Zn^{2+} , Co^{2+} , and

Cd^{2+} led to the decrease in the particle size as per SEC and DLS. Other transition metals such as Ni^{2+} and Mn^{2+} as well as the alkaline earth Ca^{2+} and Mg^{2+} did not alter the conformation of the protein N-terminal tails. Furthermore, the effect is specifically associated with the tail metal-binding site in each monomer since the substitution of aspartate 34 to an alanine residue (in the D34A variant) fully impaired the binding of metal to this site. The partial recovery to the apo-form conformation upon addition of EDTA further suggests that some divalent metals may act as modulators of the tail conformation, since the reversibility of the process is an important aspect of a putative signaling mechanism.

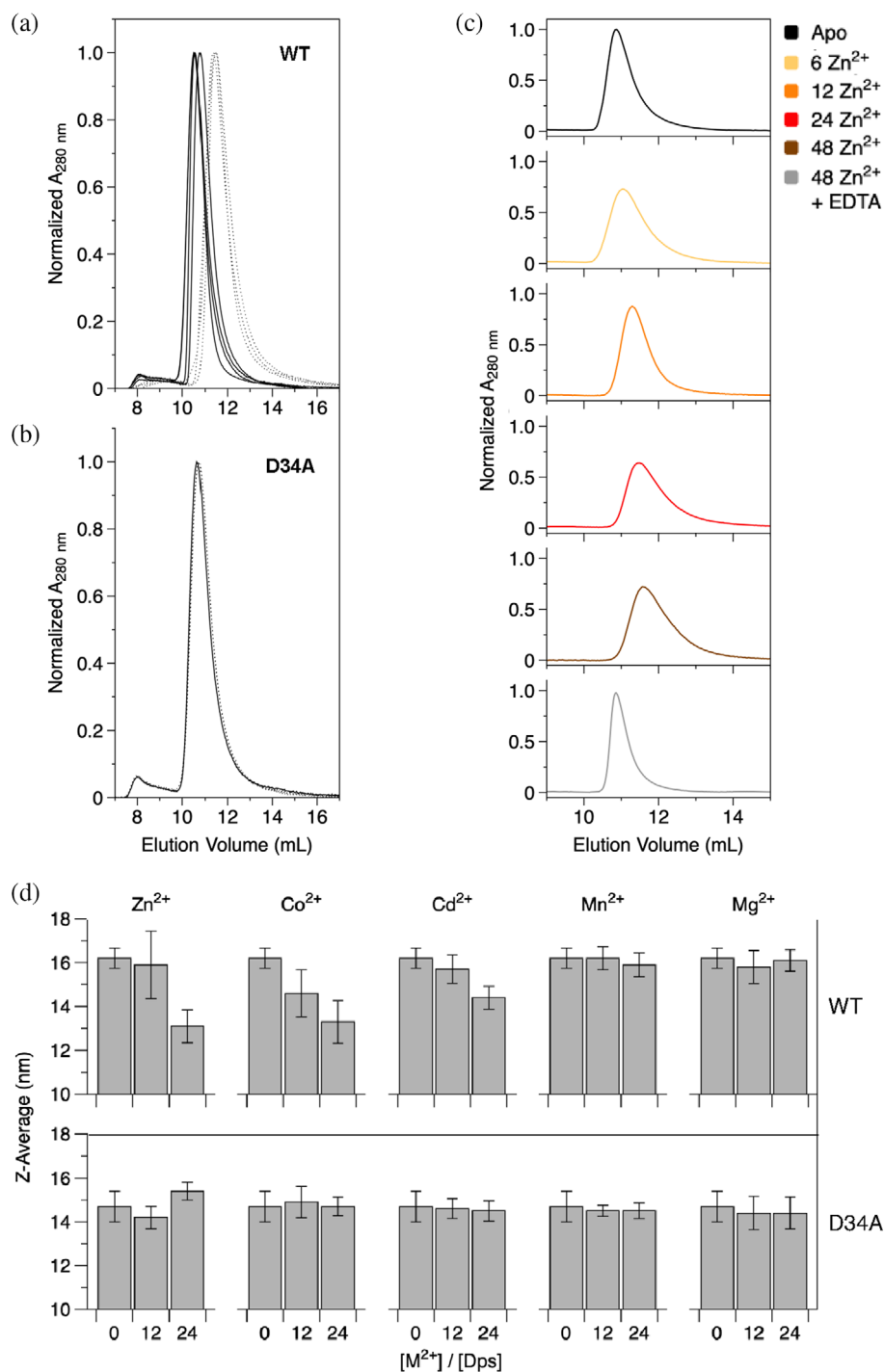
2.4 | Structural dynamics upon metal binding

A set of samples of DgrDps WT and D34A reacted with different equivalents of Zn^{2+} , Co^{2+} , and Mn^{2+} ions were prepared and analyzed using SAXS coupled to an online SEC system (Blanchet et al. 2015).

For simplicity, the datasets obtained were split into two sets: a first dataset for the analysis of the impact of adding increasing amounts of Zn^{2+} to the protein (0, 6, 12, 24, and 48 Zn^{2+} ions per protein), and a second dataset in which the structural effect of different metals (addition of 24 Zn^{2+} , Co^{2+} , or Mn^{2+} per protein) were probed, comparing both with the results obtained for the apo-form of DgrDps WT and D34A variant.

The scattering profiles of all samples (Figure 6a) are similar and consistent with a particle with a hollow sphere shape (Svergun and Koch 2003) and present a good signal-to-noise ratio up to $s = 2 \text{ nm}^{-1}$, although the noise increases in some samples (24, 48 Zn^{2+} , and 24 Co^{2+} per DgrDps WT). The proper folding and

FIGURE 4 Macromolecular properties of DgrDps WT and D34A after addition of different divalent metals. SEC elution profiles of DgrDps WT reacted with 24 equivalents of Zn^{2+} , Co^{2+} , and Cd^{2+} (dotted lines) or Ni^{2+} , Mn^{2+} , Ca^{2+} , and Mg^{2+} (full lines); (b) SEC elution profiles of DgrDps D34A incubated with 24 equivalents of Zn^{2+} , Co^{2+} , Cd^{2+} (dotted lines), and Mn^{2+} (full line); (c) Elution profiles of DgrDps WT after addition of 0 (apo, black line), 6, 12, 24, or 48 Zn^{2+} per protein (from yellow to brown, top to bottom) and EDTA to a sample pre-incubated with 48 Zn^{2+} (gray line); (d) Particle size analysis by DLS. Hydrodynamic diameter (Z-Average) of DgrDps WT (top row) and D34A (bottom row) incubated with 0, 12, and 24 equivalents of Zn^{2+} , Co^{2+} , Cd^{2+} , Mn^{2+} , or Mg^{2+} ions.



globular shape of the protein in every sample tested is confirmed by the Kratky plots (shown in Figures S2 and S3), which display the characteristic consecutive bell-shaped Gaussian curves with decreasing intensity. Guinier analysis of the scattering data (Figure 6b,d) shows good linearity and small deviations at very low s^2 values (below 0.005 nm^{-2}) for all samples, indicative of low levels of aggregation or radiation damage. The radius of gyration (R_g) determined from the Guinier plots was affected by the presence of Zn^{2+} ions, decreasing from

4.46 ± 0.01 to 4.15 ± 0.01 nm with increasing Zn^{2+} concentrations. A similar reduction in R_g was detected for the 24 Co^{2+} /DgrDps WT sample, with a R_g of 4.21 ± 0.01 nm, but not in the 24 Mn^{2+} reacted sample, for which the R_g is 4.42 ± 0.01 nm. Moreover, the R_g of the WT protein loaded with 24 Zn^{2+} and subsequently incubated with EDTA reverted the R_g back to 4.49 ± 0.01 nm. Finally, the R_g of the D34A samples was calculated to be between 4.38 ± 0.01 and 4.51 ± 0.01 nm, regardless of the divalent metal added to this protein variant.

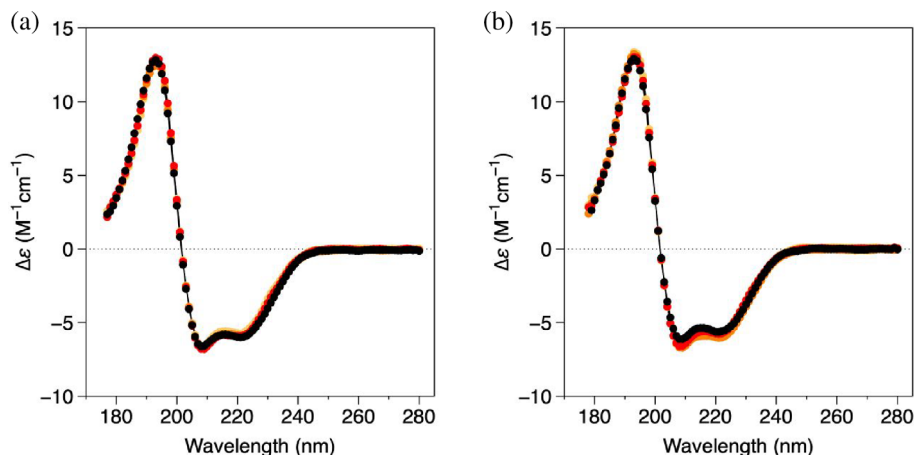


FIGURE 5 Secondary structure assessment of DgrDps WT and D34A after incubation with different concentrations of Zn^{2+} . Circular dichroism spectra of (a) WT and (b) D34A samples obtained after incubation with 0 (apo, in black), 6 (yellow), 12 (orange), and 24 (red) equivalents of Zn^{2+} per protein, in 10 mM MOPS pH 7.0, 240 mM NaF. Solid lines represent spectral reconstructed data from DichroWeb analysis.

The SAXS datasets were further analyzed using GNOM to obtain the pair distance distribution functions (Svergun 1992). All $P(r)$ plots (Figure 6c,e) display slightly asymmetrical bell-shaped curves with maximum frequency at ~ 5.8 nm for all conditions tested, with a sharp decay until ~ 10 nm, characteristic of a spherical protein with a hollow core, with an additional set of bands between 10 and 20 nm corresponding to the N-terminal tails with lower $P(r)$ values and varying D_{max} , similar to the $P(r)$ functions previously observed when studying the effect of the ionic strength (Guerra et al. 2022). The D_{max} of the apo-forms of DgrDps WT and D34A in this experiment was determined as 20.0 and 19.8 nm (black lines). As the concentration of Zn^{2+} ions added increases (Figure 6c, yellow to brown) the D_{max} gradually decreased to 14.1 nm for the 24 Zn^{2+} /protein and 14.4 nm for the 48 Zn^{2+} /protein DgrDps WT samples. The addition of EDTA after incubation with 24 equivalents of Zn^{2+} reverted the D_{max} back to 19.5 nm (gray line). However, the D_{max} of the corresponding DgrDps D34A samples was not significantly affected by the addition of either 24 and 48 Zn^{2+} per protein, varying between 19 and 21 nm. Regarding the effect of the different divalent metals, the addition of 24 Co^{2+} equivalents to DgrDps WT or D34A proteins induced an effect similar to the incubation with 24 Zn^{2+} (Figure 6e, blue lines), with a D_{max} of 13.9 nm for the WT and 20.6 nm for the D34A variant. Conversely, the $P(r)$ curves of the proteins reacted with 24 Mn^{2+} ions per protein (green lines) were analogous to the respective apo-forms, with a D_{max} value of 19.3 nm for the WT protein and 19.5 nm for the D34A variant.

The R_g values deriving from $P(r)$ calculation by GNOM are consistent with the Guinier linearization, varying between 4.52 ± 0.01 and 4.11 ± 0.01 nm for the DgrDps WT and between 4.60 ± 0.01 and 4.46 ± 0.01 nm for the D34A variant. These results are summarized in Table 2.

The low-resolution molecular envelopes of DgrDps WT and D34A proteins incubated with the different divalent metals were obtained using the ab initio modeling tool GASBOR. Representative models that best fit the experimental data are shown in Figure 7a, superimposed with the three-dimensional homology model for DgrDps as template. The end-to-end diameter of each model can be found in Table 2. All models exhibit a spherical core, ~ 10 nm wide, representing the dodecamer cage and additional variable shapes at the outer regions of the molecule. The molecular map of the apo-DgrDps WT represents the expected extended conformation previously described for higher buffer ionic strength conditions (Guerra et al. 2022), with the N-terminal tails protruding outwards in a star-like shape, with an end-to-end diameter of ~ 17.5 nm (as measured using ChimeraX [Pettersen et al. 2021]). As the amount of added Zn^{2+} increases the maps show the gradual decrease in D_{max} , displaying the tails with shorter length and more compact conformations (Figure 7b). The apparent maximum effect is achieved when 24 Zn^{2+} /protein were added, since the maps of the 24 and 48 Zn^{2+} per protein samples are almost identical with an end-to-end-diameter of ~ 14 nm. A similar shape is observed in the molecular map of the sample with 24 Co^{2+} per protein, but not in the one with 24 Mn^{2+} per protein, which resembles the conformation of the apo-form, illustrating the lack of interaction between the protein and this metal. The addition of EDTA to a sample previously incubated with 24 Zn^{2+} ions per protein generated the extended conformation, thus demonstrating the reversibility of the process. The molecular maps of DgrDps D34A, all similar to the apo-form, fully support that the conformational dynamics observed in the WT protein is triggered by the binding of some metals (Zn^{2+} and Co^{2+} ions) to the binding site present at the N-terminal tails. In these cases, the extended conformation with a diameter of ~ 17.5 nm was obtained regardless of the condition tested.

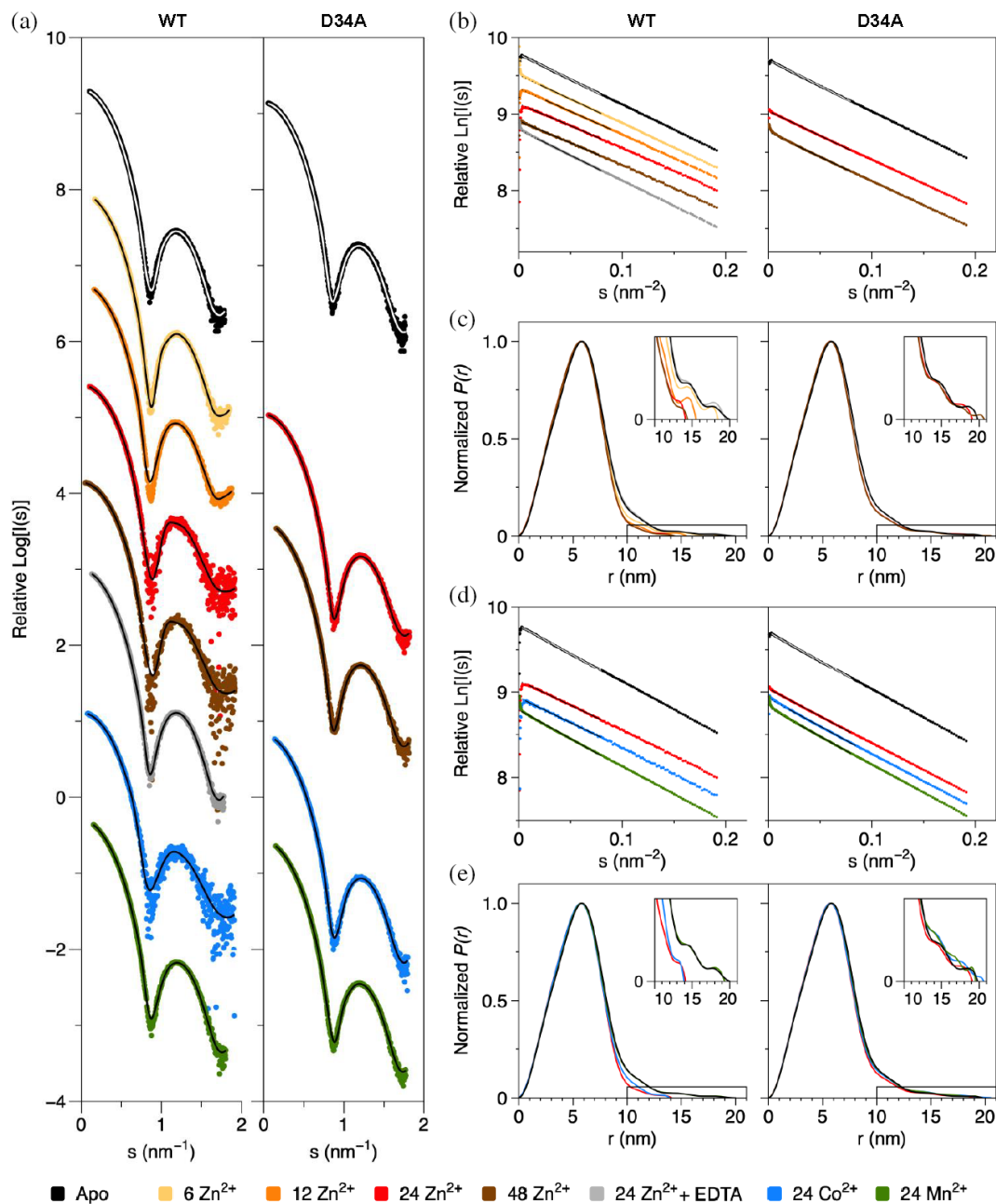


FIGURE 6 SAXS data and analysis of DgrDps WT and D34A after incubation with different divalent metals. (a) Experimental scattering curves and computed GASBOR fits (solid lines) of the apo-form of DgrDps WT and D34A samples (black) and after incubation with a metal/protein molar ratio of 6 (yellow), 12 (orange), 24 (red), and 48 Zn $^{2+}$ (brown), 24 Zn $^{2+}$ and EDTA (gray), 24 Co $^{2+}$ (blue) and 24 Mn $^{2+}$ (green) in 50 mM MOPS pH 7.0, 230 mM NaCl; (b) and (d) Guinier plots and linear fits (solid lines on top) of the scattering profiles; (c) and (e) Pair distance distribution curves; the insets are magnifications of the $P(r)$ region between 10 and 20 nm.

Considering the limitations of *ab initio* methods such as GASBOR in modeling intrinsically disordered or flexible regions, the interpretation of the models shown in Figure 7 (and the impact of divalent metal binding on the conformation of the tails) was validated using the hybrid modeling method CORAL. A tailless protein model (ΔN) (Guerra et al. 2022) was used as a fixed dodecamer structure to which 12 flexible N-terminal regions with

46 dummy residues were added. Representative models that best fit the experimental scattering profiles of DgrDps WT in the absence and presence of 24 Zn $^{2+}$ per protein are shown in Figure 8a,b. The models obtained for other samples can be found in the SASBDB. The CORAL models agree with the *ab initio* models and further illustrate the tail compacting effect caused by divalent metal binding, as the generally extended tails shown

TABLE 2 Data collection and SAXS parameters for the DgrDps WT and D34A protein samples upon incubation with different divalent metals

	WT					D34A							
	Apo ^a	6 Zn ²⁺	12 Zn ²⁺	24 Zn ²⁺	48 Zn ²⁺	EDTA	24 Co ²⁺	24 Mn ²⁺	Apo	24 Zn ²⁺	48 Zn ²⁺	24 Co ²⁺	24 Mn ²⁺
Data collection													
Beamline	P12, DESY												
Beam dimensions (mm)	0.2 × 0.05												
Detector	Pilatus 6 M												
Wavelength (Å)	1.24												
q range (nm ⁻¹)	0.05–7.0												
Concentration (mg/mL, SEC)	10	10	10	5	5	10	5	10	10	10	10	10	10
Exposure time per frame (s)	1												
Structural parameters													
$I(0)$ from Guinier	7728 (3)	9782 (4)	4697 (3)	1561 (2)	1665 (1)	10,259 (6)	1042 (1)	10,085 (6)	7291 (3)	10,205 (4)	10,779 (4)	10,361 (6)	11,568 (6)
R_g from Guinier (nm)	4.46 (1)	4.40 (1)	4.19 (1)	4.16 (1)	4.15 (1)	4.49 (1)	4.21 (1)	4.42 (1)	4.51 (1)	4.39 (1)	4.38 (1)	4.45 (1)	4.50 (1)
$I(0)$ from $P(r)$	7748 (5)	9755 (4)	4697 (3)	1555 (1)	1662 (2)	10,300 (7)	1040 (1)	10,140 (8)	7312 (4)	10,230 (4)	10,810 (6)	10,440 (10)	11,620 (8)
R_g from $P(r)$ (nm)	4.52 (1)	4.37 (1)	4.18 (1)	4.11 (1)	4.11 (1)	4.57 (1)	4.17 (1)	4.51 (1)	4.58 (1)	4.46 (1)	4.46 (1)	4.58 (1)	4.60 (1)
D_{max} from $P(r)$ (nm)	20.04	18.44	15.51	14.11	14.40	19.46	13.93	19.34	19.80	19.10	20.7	20.62	19.51
Porod volume (AutoRG) (nm ³)	447.4	421.6	394.2	351.3	367.5	440.2	343.1	434.4	449.9	408.7	408.7	411.3	438.3
Porod volume (GNOM) (nm ³)	454.1	439.2	464.1	438.6	427.9	452.9	458.0	438.0	451.3	412.8	409.1	404.5	431.0
Molecular mass (kDa)													
Estimation from data	318.5	242.6	242.6	242.6	242.6	318.5	242.6	242.6	318.5	242.6	242.6	242.6	318.4
Theoretical dodecamer	270.4	—	—	—	—	—	—	—	269.9	—	—	—	—
Modeling													
GASBOR χ^2	6.91	21.06	6.99	1.90	1.90	10.84	1.78	7.79	6.81	9.44	22.53	12.95	17.68
GASBOR Model Diameter (nm)	17.4	16.5	15.8	14.1	14.3	17.4	14.5	17.5	17.6	17.2	17.6	17.4	17.5
CORAL χ^2	3.67	6.41	4.37	1.81	1.35	3.99	1.70	4.84	2.78	3.92	4.43	4.16	6.68
Software													
1D data processing	PRIMUS												
$P(r)$ analysis	GNOM												
Ab initio methods	GASBOR												
Hybrid methods	CORAL												
Computation of model intensities	CRY SOL												
3D model visualization	ChimeraX												

Note: Values in brackets are uncertainties of the last digits.

^aApo represents the 0 M²⁺/Dps sample.

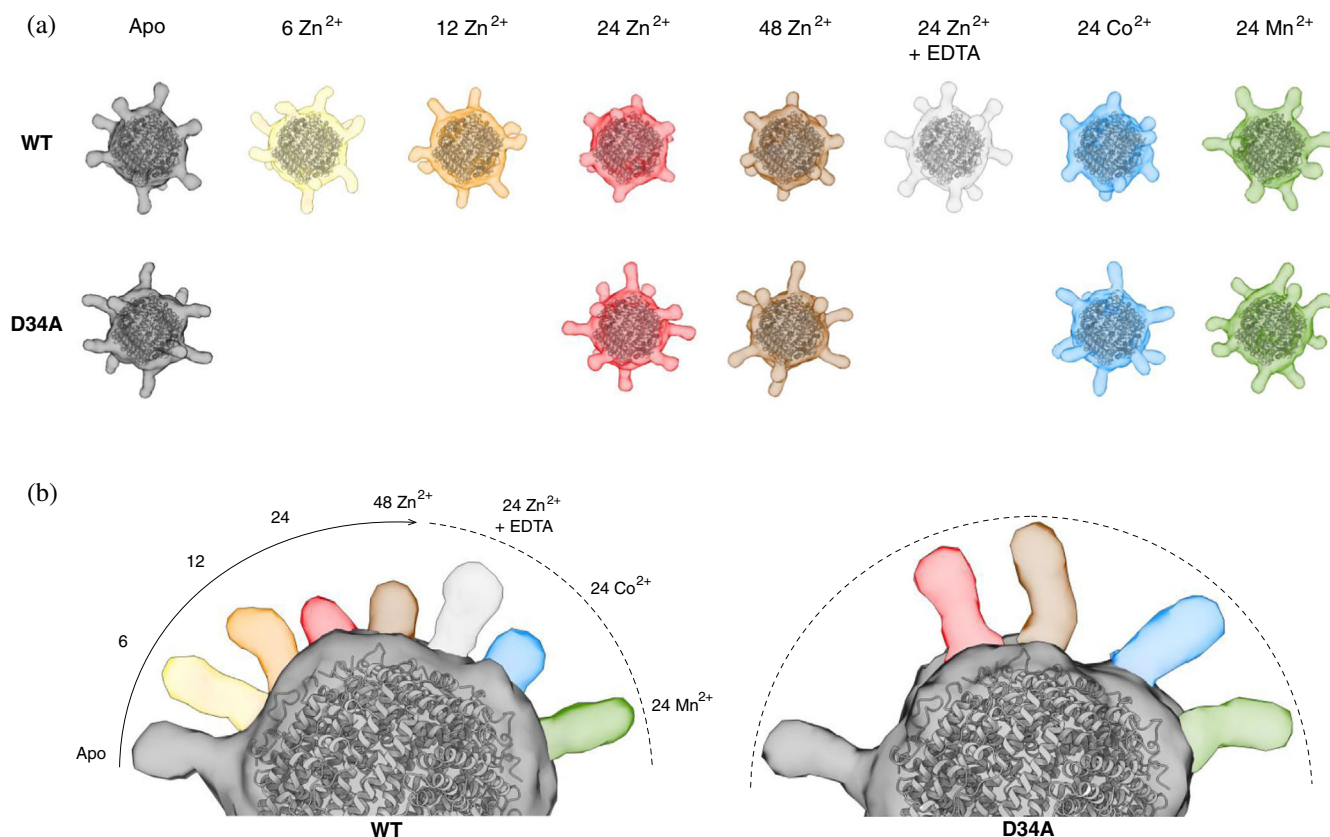


FIGURE 7 Representative ab initio models of DgrDps WT and D34A reacted with different divalent metals. (a) Molecular maps generated by GASBOR from each SAXS dataset, according to the legend on top, superimposed to the dodecamer model of the protein (gray ribbons); (b) Representative side-by-side comparison of the tails from the molecular maps shown in (a).

in the model of the apo-form (in black) were modeled pressed against the cage in the sample with 24 Zn²⁺ equivalents. Moreover, the contribution of zinc atoms present in the DgrDps structure in the scattering signal was estimated using CRY SOL. Figure 8c displays the theoretical solution scattering obtained with and without addition of 24 Zn²⁺ atoms to the CORAL model shown in Figure 8a (solid and dashed red lines). The results indicate that the contribution of zinc scattering to the scattering datasets obtained (and subsequent interference with modeling methods) is negligible.

3 | DISCUSSION

The interaction between Dps proteins and non-iron metals is a relevant topic in both fundamental and translational research on this subfamily of proteins and most frequently occurs at the ferroxidase centers or along the protein channels (in transit to and from the active sites). Interestingly, the proximal end of the N-terminal tails of *Deinococcus radiodurans* Dps1 and *Lactococcus lactis* DpsA and DpsB, as well as the C-terminal tails of

D. radiodurans Dps2 exhibit additional metal-binding sites, by crystallization with Zn²⁺, Mn²⁺, Mg²⁺, and Co²⁺ ions (Kim et al. 2006; Cuyper et al. 2007; Romão et al. 2006; Stillman et al. 2005).

A putative binding site identical to the one in *D. radiodurans* Dps1 exists in the *D. grandis* Dps monomers, according to sequence alignments and structure modeling bioinformatics. The impact of a point mutation, D34A, was investigated. SEC and DLS data in varying ionic strength conditions, confirmed that the DgrDps D34A exhibited a behavior similar to the WT protein, undergoing a conformational change, even though the metal-binding site was impaired.

Analysis of the anaerobic titration of the iron binding sites in DgrDps D34A using Mössbauer spectroscopy revealed that the high-spin ferrous species previously detected in DgrDps WT (with parameters $\delta = 1.10 \pm 0.02$ mm/s, $\Delta E_Q = 3.82 \pm 0.02$ mm/s, therein termed Site II) was absent, leading to the conclusion that this amino acid residue is essential for iron binding. Based on bioinformatics, the metal-binding site at the proximal end of the N-terminal tails is most likely composed of residues Asp34, His37, His48, and Glu53, similar to the one

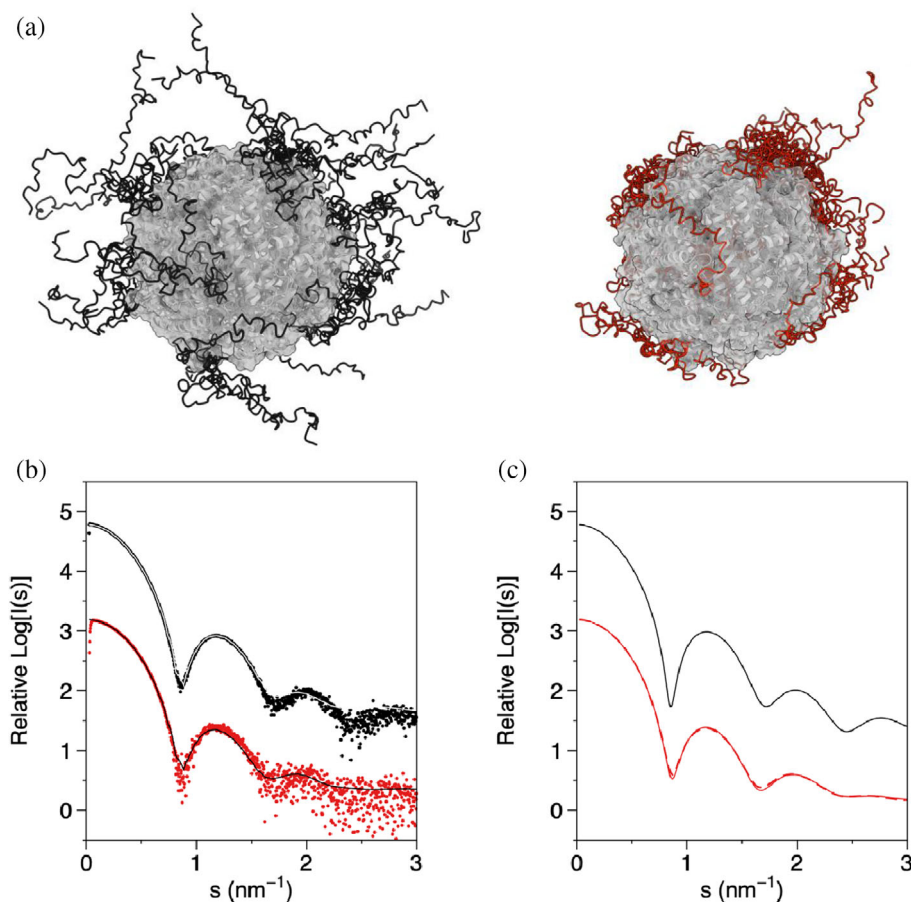


FIGURE 8 Validation of the ab initio modeling of the flexible N-terminal tails using the CORAL software. (a) Representative CORAL models of the N-terminal tails in DgrDps WT in its apo-form (black chains) and after incubation with 24 equivalents of Zn^{2+} per protein (red chains). A folded tailless dodecameric cage model was imposed as a fixed structure (in gray) with 12 flexible N-terminal tails. Each model represents five replicate CORAL models superimposed. (b) Experimental scattering profiles and computed CORAL fits (white and black solid lines) obtained for each sample. (c) Theoretical solution scattering of the CORAL models shown in (a) by CRYSOLOG. The red dashed line represents the theoretical scattering curve of the model in red with 24 Zn^{2+} atoms artificially placed in their putative binding sites.

identified in the crystal structures of *D. radiodurans* Dps1 (Kim et al. 2006; Romão et al. 2006). To the best of our knowledge in the present work, we characterize for the first time the interaction of Fe^{2+} ions to a metal-binding site involving Asp34, which hints towards the regulation of protein function between iron storage and DNA-binding by iron sensing.

Analogous to what was shown in the ionic strength dependence experiments, the specific interaction of some divalent metals with the N-terminal tails of DgrDps WT alters the macromolecular structural properties of the protein, with the Stokes radius and hydrodynamic diameter gradually decreasing for higher occupancies, without affecting the overall secondary structure of the protein. In our study, this effect was however limited to the binding of Zn^{2+} , Co^{2+} , and Cd^{2+} ions, with neither Ni^{2+} , Mn^{2+} , Mg^{2+} , nor Ca^{2+} rendering a discernible effect. The comparison with equivalent samples of the variant DgrDps D34A, in which no significant change was detected, further confirms that the effect observed is indeed due to the occupation of the binding site in each N-terminal tail.

The overall shape of the protein in different divalent metal conditions was examined using SEC-SAXS. The SAXS parameters obtained are consistent with the SEC

and DLS experiments, with the radius of gyration and maximum diameter ranging from $R_g \sim 4.5$ nm and $D_{\text{max}} \sim 20$ nm for the apo-protein to $R_g \sim 4.1$ nm and $D_{\text{max}} \sim 14$ nm for the most altered protein form. Overall, the protein conformations revealed in this experiment are similar to the extended and compact conformations previously described (Guerra et al. 2022). While the apo-protein exhibits the expected star-shaped conformation with extended tails, the N-terminal tails were gradually found in a shorter, more compact conformation in metal-bound protein forms (Zn^{2+} and Co^{2+} , but not Mn^{2+}). The extended conformation was restored upon metal chelation by EDTA. Considering the results from the Mössbauer ferrous titration experiments described here and in agreement with our previous work (Guerra et al. 2022), the saturation of this effect at 24 equivalents suggests that these metals may also interact with the FOCs, thus saturating the 12 tail binding sites in parallel with the binding to the FOCs (12 FOCs per protein), as quantified by Mössbauer spectral deconvolution. Moreover, it is likely that the binding of Fe^{2+} ions to the N-terminal binding site induces a tail compaction effect similar to Zn^{2+} and Co^{2+} . However, it should be noted that the confirmation and functional role of such is still to be experimentally demonstrated.

A similar tail-compactness effect was previously described through SAXS for the incubation of *Escherichia coli* Dps with Mg^{2+} .¹⁵ Strikingly, our results seem to contradict this observation since Mg^{2+} produced no discernible effect on DgrDps. However, this may be due to the differences in length and composition of the N-terminal tails of both *E. coli* and *D. grandis* Dps proteins. The former comprises half the number of residues and does not contain a metal-binding site. Also, previous works suggested that Mn^{2+} binds to the N-terminal binding site of *D. radiodurans* Dps1 (Nguyen and Grove 2012), which is not in agreement with the results from the DgrDps experiment herein described.

Overall, the results from this work add another layer to the conclusions gathered throughout recent years in Dps research: the conformation of the N-terminal tails of DgrDps (and thus, the structural properties of the protein) can be modulated by the presence of physiologically relevant agents, in this case through the binding of specific metal cations such as Zn^{2+} , Co^{2+} , Cd^{2+} (and likely Fe^{2+}) to the binding site present in the proximal end of the N-terminal tails. Given the reported importance of the tails in protein oligomerization and DNA-binding properties, these results inspire further investigation on the effects of metal-binding on the function of the protein.

4 | MATERIALS AND METHODS

4.1 | Protein production and purification

Recombinant expression of DgrDps WT and D34A variant proteins was achieved as described before for the DgrDps WT (Guerra et al. 2022). The expression vector for production of the D34A mutant (pET21c:DgrDpsD34A) was prepared by following a site-directed mutagenesis kit protocol (NZYTech, Lisboa, Portugal) using the pET21:DgrDpsWT as parental DNA. The two synthetic oligonucleotides (Forward 5'-CAA GCG GTG CAG CAA AAG CCG **CTG** CAG CAC ATC TGA GCA CC-3' and Reverse 5'-GGT GCT CAG ATG TGC TGC **AGC** GGC TTT TGC TGC ACC GCT TG-3') with the desired point mutation (in boldface) were designed according to the manufacturer guidelines and obtained from Eurofins Genomics (Ebersberg, Germany). Each PCR reaction contained 30 ng of parental DNA, 125 ng of each primer, dNTPs mix and 2.5 U of NZYProof DNA polymerase in the appropriate buffer, according to manufacturer guidelines. The PCR was performed in a thermocycler (Biometra, Invitrogen) following the protocol instructions using an annealing temperature of 60°C. After analysis of the efficiency of the amplification on a

1% agarose gel, the remaining PCR mixture was incubated with 5 μ L of DpnI for 1 h at 37°C for digestion of the parental template. The hydrolysis reaction products were used to transform ultracompetent *E. coli* NZYStar cells (NZYTech). To confirm the point mutation, the resulting plasmid DNA pET21c:DgrDpsD34A was sequenced (Eurofins Genomics).

The production of DgrDps D34A followed the same procedure as DgrDps WT (Guerra et al. 2022). Briefly, transformed *E. coli* BL21(DE3) cells were cultured in liquid Luria Broth (LB) media (10 g/L tryptone, 5 g/L yeast extract, 10 g/L NaCl, pH 7.0) containing 100 μ g/mL ampicillin until an $OD_{600\text{ nm}} \sim 0.7$ before induction with 0.5 mM IPTG (isopropyl- β -D-1-thiogalactopyranoside) for 3 hr at 37°C. Since the proteins were expressed as inclusion bodies, the pellet obtained after centrifugation of the cell extract was resuspended in 10 mM Tris-HCl pH 7.0, 250 mM NaCl, 1% Triton X-100 and 1 M urea for 1 hr at room temperature. The resulting supernatant obtained after a centrifugation for 30 min at 15,000g was then dialyzed against 10 mM Tris-HCl pH 7.0, 1 M urea for protein solubilization. The purification procedure was performed using an ÄKTAprime plus system (Cytiva) and included two consecutive anionic exchange and one SEC chromatographic steps. A preparative step using a DEAE Fast Flow column (Cytiva) followed by a high-resolution step using a Resource Q 6 mL pre-packed column (Cytiva). In both cases the protein was eluted using a 0–500 mM NaCl linear gradient and protein purity was assessed using SDS-PAGE. DgrDps D34A containing fractions were pooled, concentrated, and ultimately injected into a Superdex 200 Prep Grade size-exclusion chromatography column for final polishing and buffer exchange, in 200 mM MOPS pH 7.0 with 200 mM NaCl. Pure fractions were concentrated and stored at -80°C until further use.

Protein concentration of DgrDps WT or D34A stock solutions and samples was determined using the theoretical molar extinction coefficient of the protein monomer at 280 nm, equal to 21,430 $\text{M}^{-1}\text{ cm}^{-1}$ for both protein dodecamers, according to ExPASy ProtParam tool (Gasteiger et al. 2005).

4.2 | General sample preparation

DgrDps WT and D34A samples were dialyzed against 50 mM MOPS pH 7.0, 230 mM NaCl (or 10 mM MOPS pH 7.0, 240 mM NaF in the case of SRCD samples) to ensure a stable extended conformation before reaction with the different divalent metals used in this work. After incubation with different concentrations of the metals (from 6 to 48 M^{2+} /Dps dodecamer, corresponding to 0.5–

4 M^{2+} /monomer) for 20 min at room temperature, the resulting metal loaded-protein samples were centrifuged for 10 min at 15,000g before analysis. When appropriate, the metal loaded-DgrDps samples were also subsequently incubated with 5 mM ethylenediaminetetraacetate (EDTA) after incubation with the divalent metals.

The Zn^{2+} stock solution used derived from a commercial metal standard (metallic Zn dissolved in 0.5 M HNO_3). The stock solutions of the remaining divalent metals were prepared by dissolving commercial metallic salts (>98% purity, MERCK) of $CoSO_4 \cdot 7H_2O$, $Cd(NO_3)_2 \cdot 7H_2O$, $NiCl_2 \cdot 6H_2O$, $MnSO_4 \cdot H_2O$, $CaCl_2 \cdot 2H_2O$ and $MgCl_2 \cdot 6H_2O$ in H_2O at pH 2.0 (acidified with H_2SO_4).

The DgrDps D34A samples for the SEC and DLS measurements in different ionic strength conditions were prepared as described for DgrDps WT (Guerra et al. 2022).

4.3 | Molecular mass and hydrodynamic radius estimation

A high-performance Superdex 200 10/300 GL column (Cytiva) was calibrated as described before (Guerra et al. 2022). A calibration curve was prepared to determine the apparent molecular mass and hydrodynamic radius (Stokes radius, R_S) (La Verde et al. 2017):

$$\text{Log}_{10}(\text{MM}) = -1.546 \frac{V_e}{V_o} + 7.677 \text{ and}$$

$$\text{Log}_{10}(R_S) = -1.028 \frac{V_e - V_o}{V_t - V_o} + 0.99$$

where MM is the apparent molecular mass in kDa, R_S is the Stokes radius in nm, V_e is the elution volume of the protein, V_o is the void volume, and V_t is the total volume of the bed column.

The apparent molecular mass and apparent Stokes radius of DgrDps WT and D34A in different test conditions were estimated by injecting the samples on the SEC column pre-equilibrated with 50 mM MOPS pH 7.0, 230 mM NaCl at a flow rate of 0.5 mL/min.

4.4 | Dynamic light scattering analysis

Apo- and metal-loaded DgrDps samples, at 1 mg/mL protein concentration in 50 mM MOPS pH 7.0, 230 mM NaCl buffer were centrifuged for 30 min at 14,000g at room temperature prior measurement in a HORIBA SZ-100 nanoparticle analyzer equipped with a 10 mW 532 nm laser and detection at a scattering angle of 90° during 2 min at $25^\circ C$, in at least triplicates. The intensity

weighted mean hydrodynamic diameter (Z-Average) and the polydispersity index (PI) were calculated using the built-in software of the equipment, assuming a standard monodisperse form of distribution, and using a particle refractive index of 1.6 for organic sample and water settings as dispersion medium (refractive index of 1.333).

4.5 | Mössbauer spectroscopy characterization

DgrDps D34A protein samples at 166 μM in 200 mM MOPS pH 7.0, 200 mM NaCl were incubated anaerobically (inside an anaerobic glovebox, MBraun MBLab) with $^{57}FeSO_4$ at molar ratios of 6, 12, 24, and 48 Fe/Dps (ca. 1–8 mM Fe) for 20 min at room temperature and subsequently frozen in liquid nitrogen. Small Fe/protein molar ratios (moles of iron/moles of Dps dodecamer) were used, to avoid an excess of added ferrous ions. In those conditions, the N-terminal binding site will saturate as shown in a previous published work (Guerra et al. 2022). For this reason, and in accordance with previously obtained data, ferrous iron removal/cleaning procedures of the Mössbauer samples to attest the presence/absence of a tail binding site are not required. The $^{57}FeSO_4$ stock solution was prepared as described before by acidic dissolution of a ^{57}Fe metal foil (> 95% enrichment) in H_2SO_4 (Ravi et al. 1994; Penas et al. 2019) and quantified by the 1,10-phenanthroline method (Besada 1987).

Mössbauer spectra were measured at 80 K in the absence of external magnetic field in transmission mode using a conventional constant acceleration spectrometer and a ^{57}Co source in Rh matrix. The velocity scale was calibrated using an α -Fe foil at room temperature and the isomer shift values (δ) are given relative to this standard. Global spectral analysis and deconvolution were carried out taking the values of δ , ΔE_Q and linewidth as variables using the WMOSS software. Occupancy reflects the number of ferrous ions per type of binding site in each sample and was calculated by multiplying the contribution (in percentage) of each species by the amount of iron added to the protein (Fe/Dps molar ratio).

4.6 | Synchrotron radiation circular dichroism analysis

Synchrotron radiation circular dichroism (SRCD) spectra of DgrDps WT and D34A samples were acquired at the AU-CD beamline at the ASTRID2 synchrotron radiation facility (ISA, Department of Physics and Astronomy, Aarhus University, Denmark).

The spectra of 1 mg/mL protein samples in 10 mM MOPS pH 7.0, 240 mM NaF were recorded in 1 nm steps and a dwell time of 2.1 s per step, in triplicate, using a nominally 0.01 cm pathlength quartz cell (SUPRASIL, Hellma GmbH, Germany), for the wavelength range of 170–280 nm, at 25°C. The actual pathlength of the cell was determined to be 0.01008 cm by an interference technique (Hoffmann et al. 2016).

The differential molar extinction coefficient, $\Delta\epsilon$, for each spectrum was calculated using protein concentration estimated from the absorbance at 205 nm and the protein molar extinction coefficient at that wavelength (Anthis and Clore 2013). Secondary structure content of the proteins in each sample condition was estimated using DichroWeb, an online CD structure analysis tool (Miles et al. 2022), using CDSSTR as analysis program and SP175 as the reference set. DichroWeb analysis programs deconvolute the percentages of each type of secondary structure (helix, strand, turns, or unordered) present in a sample by simulating each experimental spectrum using the reference spectra of over 70 proteins (in the case of the SP175 reference dataset).

4.7 | Small-angle X-ray scattering analysis

Synchrotron SAXS data was measured at beamline P12 operated by the European Molecular Biology Laboratory, EMBL, at the PETRA III storage ring (Blanchet et al. 2015) (DESY, Hamburg, Germany). The scattering intensity, $I(s)$, was recorded in a momentum transfer range between 0.05 and 7.0 nm⁻¹, with $s = (4\pi\sin 2\theta)/\lambda$, in which 2θ is the scattering angle and λ the X-ray wavelength and equal to 0.124 nm. Scattered X-ray photons were detected on a Pilatus 6 M detector (DECTRIS, Switzerland) distancing 3 m from the sample.

DgrDps WT and D34A samples at ~10 mg/mL initial concentration were measured by SEC-SAXS (Graewert et al. 2015) using a Superdex 200 Increase 5/150 GL column (Cytiva) in buffer containing 50 mM MOPS pH 7.0, 230 mM NaCl. The 2D images were radially averaged, frames with no trace of radiation damage were averaged and used for the analysis. In SEC-SAXS data collection, 3000 successive frames of 1 s were measured during the chromatographic separation. CHROMIXS (Panjkovich and Svergun 2018) was used to visualize the SEC-SAXS data and select relevant sample and buffer frames. Data were reduced using the SASflow pipeline (Franke et al. 2012).

The one-dimensional datasets were analyzed and treated using standard protocols and the ATSAS program suite (Manalastas-Cantos et al. 2021) (CHROMIX,

PRIMUS, GNOM). The scattering profiles, Guinier plots, Kratky plots are used to determine the R_g and $I(0)$, evaluate the quality of the dataset, assess protein monodispersity, and to estimate the molecular mass and Porod volume of the particle in solution. The pair distance distribution ($P(r)$) calculations (including R_g , $I(0)$ and D_{max}) from each scattering profile were performed using GNOM, an indirect transform program for small-angle scattering data processing. The ab initio models of DgrDps WT and D34A were obtained from the SAXS data using GASBOR (Svergun et al. 2001), a program for ab initio reconstruction of protein structure from a chain-like ensemble of dummy residues, using P23 symmetry and 205 dummy residues per asymmetric part as restrictions. At least 10 independent iterations of the program were performed per sample and a representative of the most typical result obtained for each condition was used to prepare the three-dimensional molecular maps shown in Figure 7. The molecular maps were rendered using ChimeraX (Pettersen et al. 2021) and superimposed on a protein model of the DgrDps dodecamer obtained through homology modeling (Waterhouse et al. 2018) using the structure of *D. radiodurans* Dps1 (PDB 2C2U) as the template. The N-terminal tails were further modeled as flexible chains using CORAL (Petoukhov et al. 2012), for validation of the GASBOR ab initio modeling. CORAL is a hybrid method that performs rigid body modeling of rigid protein domains with unrigid fragments such as termini. To better reflect the inherent flexibility of the termini in each sample, a pre-generated library of self-avoiding random loops composed of dummy residues is computed, sampling 20 random structures for every possible end-to-end distance in each dataset. In this case, a tailless model of the DgrDps dodecamer was used as a fixed structure (P1 symmetry) with 12 additional flexible N-terminal fragments with 46 dummy residues each. Furthermore, and to confirm that the presence of Zn²⁺ was not significantly contributing to the scattering signal, the theoretical intensities of the resulting protein models both with and without Zn atoms (12 Zn²⁺ atoms placed at the N-terminal binding site and 12 Zn²⁺ at the FOCs in the protein model), were calculated using CRY SOL (Franke et al. 2017), which calculates the solution scattering of atomic protein structures (including ligands) and fits it to an experimental dataset.

AUTHOR CONTRIBUTIONS

João P.L. Guerra: Conceptualization (equal); formal analysis (equal); investigation (lead); writing – original draft (equal); writing – review and editing (equal). **Clement E. Blanchet:** Formal analysis (equal); investigation

(equal); methodology (equal); resources (equal); writing – review and editing (equal). **Bruno J.C. Vieira:** Investigation (equal); methodology (equal); resources (equal); writing – review and editing (equal). **João C. Waerenborgh:** Methodology (equal); resources (equal); writing – review and editing (equal). **Nykola C. Jones:** Methodology (equal); resources (equal); writing – review and editing (equal). **Søren Vronning Hoffmann:** Methodology (equal); resources (equal); writing – review and editing (equal). **Alice S. Pereira:** Conceptualization (lead); formal analysis (lead); funding acquisition (lead); investigation (lead); methodology (lead); project administration (lead); resources (lead); supervision (lead); writing – review and editing (lead). **Pedro Tavares:** Conceptualization (lead); formal analysis (lead); funding acquisition (lead); investigation (lead); methodology (lead); project administration (lead); resources (lead); supervision (lead); writing – review and editing (lead).

ACKNOWLEDGMENTS

This work was financed by national funds from FCT—Fundação para a Ciência e a Tecnologia (FCT-MCTES), I.P., in the scope of project UIDB/04378/2020 of the Research Unit on Applied Molecular Biosciences—UCIBIO, project LA/P/0140/2020 of the Associate Laboratory Institute for Health and Bioeconomy—i4HB and project UID/Multi/04349/2019 of the Center for Nuclear Sciences and Technologies (C2TN), as well as the National Infrastructure Roadmap, LTHMFL-NECL, LISBOA-01-0145-FEDER-022096. This research was supported by the FCT-MCTES grants PTDC/BIA-PRO/111485/2009 (to P.T.) and PTDC/QUI/64248/2006 (to A.S.P.). This work was also supported by the Radiation Biology and Biophysics Doctoral Training Programme (RaBBiT, PD/00193/2012—UCIBIO (UIDB/04378/2020), CEFITEC (UIDB/00068/2020)), all financed by national funds from FCT-MCTES. J.P.L.G. was supported by the Radiation Biology and Biophysics Doctoral Training Programme and FCT-MCTES, Ph.D. Fellowships (PD/BD/135476/2017 and COVID/BD/152497/2022). This work benefited from funding by the project CALIPSOplus, under the Grant Agreement 730872 from the EU Framework Programme for Research and Innovation HORIZON 2020.

CONFLICT OF INTEREST STATEMENT

The authors declare no conflict of interest.


DATA AVAILABILITY STATEMENT

The data that support the findings of this study are available from the corresponding author upon reasonable request.

ORCID

João P. L. Guerra  <https://orcid.org/0000-0001-5441-9446>

Clement E. Blanchet  <https://orcid.org/0000-0003-3432-8496>

Bruno J. C. Vieira  <https://orcid.org/0000-0002-6536-9875>

João C. Waerenborgh  <https://orcid.org/0000-0001-6171-4099>

Nykola C. Jones  <https://orcid.org/0000-0002-4081-6405>

Søren Vronning Hoffmann  <https://orcid.org/0000-0002-8018-5433>

Alice S. Pereira  <https://orcid.org/0000-0001-5567-6073>

Pedro Tavares  <https://orcid.org/0000-0002-7398-2661>

REFERENCES

- Alaleona F, Franceschini S, Ceci P, Ilari A, Chiancone E. *Thermosynechococcus elongatus* DpsA binds Zn(II) at a unique three histidine-containing ferroxidase center and utilizes O₂ as iron oxidant with very high efficiency, unlike the typical Dps proteins. *FEBS J.* 2010;277:903–17. <https://doi.org/10.1111/j.1742-4658.2009.07532.x>
- Anthis NJ, Clore GM. Sequence-specific determination of protein and peptide concentrations by absorbance at 205 nm. *Protein Sci.* 2013;22:851–8. <https://doi.org/10.1002/pro.2253>
- Besada A. A facile and sensitive spectrophotometric determination of ascorbic acid. *Talanta.* 1987;34:731–2.
- Bhattacharyya G, Grove A. The N-terminal extensions of *Deinococcus radiodurans* Dps-1 mediate DNA major groove interactions as well as assembly of the dodecamer. *J Biol Chem.* 2007;282:11921–30.
- Blanchet CE, Spilotos A, Schwemmer F, Graewert MA, Kikhney A, Jeffries CM, et al. Versatile sample environments and automation for biological solution X-ray scattering experiments at the P12 beamline (PETRA III, DESY). *J Appl Cryst.* 2015;48:431–43.
- Bozzi M, Mignogna G, Stefanini S, Barra D, Longhi C, Valenti P, et al. A novel non-heme iron-binding ferritin related to the DNA-binding proteins of the Dps family in *listeria innocua*. *J Biol Chem.* 1997;272:3259–65.
- Ceci P, Cellai S, Falvo E, Rivetti C, Rossi GL, Chiancone E. DNA condensation and self-aggregation of *Escherichia coli* Dps are coupled phenomena related to the properties of the N-terminus. *Nucleic Acids Res.* 2004;32:5935–44. <https://doi.org/10.1093/nar/gkh915>
- Crichton RR, Declercq J-P. X-ray structures of ferritins and related proteins. *Biochim Biophys Acta.* 2010;1800:706–18. <https://doi.org/10.1016/j.bbagen.2010.03.019>
- Cuypers MG, Mitchell EP, Romão CV, McSweeney SM. The crystal structure of the Dps2 from *Deinococcus radiodurans* reveals an unusual pore profile with a non-specific metal binding site. *J Mol Biol.* 2007;371:787–99.
- Dadinova L, Kamyshinsky R, Chesnokov Y, Mozhaev A, Matveev V, Gruzinov A, et al. Structural rearrangement of Dps-DNA complex caused by divalent Mg and Fe cations. *Int J Mol Sci.* 2021;22:6056.
- Dubrovin EV, Dadinova LA, Petoukhov MV, Soshinskaya EY, Mozhaev AA, Klinov DV, et al. Spatial organization of Dps and DNA-Dps complexes. *J Mol Biol.* 2021;433:166930.

- Franke D, Kikhney AG, Svergun DI. Automated acquisition and analysis of small angle X-ray scattering data. *Nucl Instrum Methods Phys Res Sect A Accel Spectrometers Detect Assoc Equip.* 2012;689:52–9. <https://doi.org/10.1016/j.nima.2012.06.008>
- Franke D, Petoukhov MV, Konarev PV, Panjkovich A, Tuukkanen A, Mertens HDT, et al. ATSAS 2.8: a comprehensive data analysis suite for small-angle scattering from macromolecular solutions. *J Appl Cryst.* 2017;50:1212–25.
- Gasteiger E, Hoogland C, Gattiker A, Duvaud S, Wilkins MR, Appel RD, et al. Protein identification and analysis tools on the ExPASy server. In: Walker JM, editor. *The proteomics protocols handbook*. NJ, USA: Springer Protocols Handbooks, Humana Press; 2005. p. 571–607.
- Graewert MA, Franke D, Jeffries CM, Blanchet CE, Ruskule D, Kuhle K, et al. Automated pipeline for purification, biophysical and X-ray analysis of biomacromolecular solutions. *Sci Rep.* 2015;5:10734.
- Grant RA, Filman DJ, Finkel SE, Kolter R, Hogle JM. The crystal structure of Dps, a ferritin homolog that binds and protects DNA. *Nat Struct Biol.* 1998;5:294–303. <https://doi.org/10.1038/nsb0498-294>
- Guerra JPL, Jacinto JP, Tavares P. Miniferritins: small multifunctional protein cages. *Coord Chem Rev.* 2021;449:214187.
- Guerra JPL, Blanchet CE, Vieira BJC, Almeida AV, Waerenborgh JC, Jones NC, et al. The conformation of the N-terminal tails of *Deinococcus grandis* Dps is modulated by the ionic strength. *Int J Mol Sci.* 2022;23:4871.
- Haikarainen T, Thanassoulas A, Stavros P, Nounesis G, Haataja S, Papageorgiou AC. Structural and thermodynamic characterization of metal ion binding in *Streptococcus suis* Dpr. *J Mol Biol.* 2011;405:448–60.
- Hoffmann SV, Fano M, van de Weert M. Circular dichroism spectroscopy for structural characterization of proteins. In: Müllertz A, Perrie Y, Rades T, editors. *Analytical techniques in the pharmaceutical sciences. Advances in delivery science and technology*. New York: Springer; 2016. p. 223–51. https://doi.org/10.1007/978-1-4939-4029-5_6
- Huergo LF, Rahman H, Ibrahimovic A, Day CJ, Korolik V. *Campylobacter jejuni* Dps protein binds DNA in the presence of iron or hydrogen peroxide. *J Bacteriol.* 2013;195:1970–8. <https://doi.org/10.1128/JB.00059-13>
- Jacinto JP, Penas D, Guerra JPL, Almeida AV, Jones NC, Hoffmann SV, et al. Dps–DNA interaction in *Marinobacter hydrocarbonoclasticus* protein: effect of a single-charge alteration. *Eur Biophys J.* 2021;50:513–21. <https://doi.org/10.1007/s00249-021-01538-0>
- Karas VO, Westerlaken I, Meyer AS. The DNA-binding protein from starved cells (Dps) utilizes dual functions to defend cells against multiple stresses. *J Bacteriol.* 2015;197:3206–15. <https://doi.org/10.1128/JB.00475-15>
- Kim S-G, Bhattacharyya G, Grove A, Lee Y-H. Crystal structure of Dps-1, a functionally distinct Dps protein from *Deinococcus radiodurans*. *J Mol Biol.* 2006;361:105–14.
- La Verde V, Dominici P, Astegno A. Determination of hydrodynamic radius of proteins by size exclusion chromatography. *Bio Protoc.* 2017;7:1–14.
- Lee SY, Lim CJ, Dröge P, Yan J. Regulation of bacterial DNA packaging in early stationary phase by competitive DNA binding of Dps and IHF. *Sci Rep.* 2015;5:1–10.
- Manalastas-Cantos K, Konarev PV, Hajizadeh NR, Kikhney AG, Petoukhov MV, Molodenskiy DS, et al. ATSAS 3.0: expanded functionality and new tools for small-angle scattering data analysis. *J Appl Cryst.* 2021;54:343–55.
- Miles AJ, Ramalli SG, Wallace BA. DichroWeb, a website for calculating protein secondary structure from circular dichroism spectroscopic data. *Protein Sci.* 2022;31:37–46. <https://doi.org/10.1002/pro.4153>
- Nguyen KH, Grove A. Metal binding at the *Deinococcus radiodurans* Dps-1 N-terminal metal site controls dodecameric assembly and DNA binding. *Biochemistry.* 2012;51:6679–89. <https://doi.org/10.1021/bi300703x>
- Panjkovich A, Svergun DI. CHROMIXS: automatic and interactive analysis of chromatography-coupled small-angle X-ray scattering data. *Bioinformatics.* 2018;34:1944–6.
- Papinutto E, Dundon WG, Pitulis N, Battistutta R, Montecucco C, Zanotti G. Structure of two iron-binding proteins from *Bacillus anthracis*. *J Biol Chem.* 2002;277:15093–8. <https://doi.org/10.1074/jbc.M112378200>
- Penas D, Pereira AS, Tavares P. Direct evidence for ferrous ion oxidation and incorporation in the absence of oxidants by Dps from *Marinobacter hydrocarbonoclasticus*. *Angew Chemie Int Ed.* 2019;58:1013–8. <https://doi.org/10.1002/anie.201809584>
- Petoukhov MV, Franke D, Shkumatov AV, Tria G, Kikhney AG, Gajda M, et al. New developments in the ATSAS program package for small-angle scattering data analysis. *J Appl Cryst.* 2012; 45:342–50.
- Pettersen EF, Goddard TD, Huang CC, Meng EC, Couch GS, Croll TI, et al. UCSF ChimeraX: structure visualization for researchers, educators, and developers. *Protein Sci.* 2021;30:70–82. <https://doi.org/10.1002/pro.3943>
- Ravi N, Bollinger JM, Huynh BH, Stubbe JA, Edmondson DE, Bollinger JM, et al. Mechanism of assembly of the tyrosyl radical-diiron(III) cofactor of *E. coli* ribonucleotide reductase. 1. Mössbauer characterization of the diferric radical precursor. *J Am Chem Soc.* 1994;116:8007–14.
- Romão CV, Mitchell EP, McSweeney S. The crystal structure of *Deinococcus radiodurans* Dps protein (DR2263) reveals the presence of a novel metal Centre in the N terminus. *J Biol Inorg Chem.* 2006;11:891–902. <https://doi.org/10.1007/s00775-006-0142-5>
- Roy S, Saraswathi R, Gupta S, Sekar K, Chatterji D, Vijayan M. Role of N and C-terminal tails in DNA binding and assembly in Dps: structural studies of *Mycobacterium smegmatis* Dps deletion mutants. *J Mol Biol.* 2007;370:752–67.
- Santos SP, Cuyppers MG, Round A, Finet S, Narayanan T, Mitchell EP, et al. SAXS structural studies of Dps from *Deinococcus radiodurans* highlights the conformation of the mobile N-terminal extensions. *J Mol Biol.* 2017;429:667–87.
- Soshinskaya EY, Dadinova LA, Mozhaev AA, Shtykova EV. Effect of buffer composition on conformational flexibility of N-terminal fragments of Dps and the nature of interactions with DNA. *Small-Angle X-Ray Scattering Study. Crystallogr Rep.* 2020;65:891–9. <https://doi.org/10.1134/S1063774520060334>
- Stetefeld J, McKenna SA, Patel TR. Dynamic light scattering: a practical guide and applications in biomedical sciences. *Biophys Rev.* 2016;8:409–27. <https://doi.org/10.1007/s12551-016-0218-6>
- Stillman TJ, Upadhyay M, Norte VA, Sedelnikova SE, Carradus M, Tzokov S, et al. The crystal structures of

- Lactococcus lactis* MG1363 Dps proteins reveal the presence of an N-terminal helix that is required for DNA binding. *Mol Microbiol.* 2005;57:1101–12. <https://doi.org/10.1111/j.1365-2958.2005.04757.x>
- Svergun DI. Determination of the regularization parameter in indirect-transform methods using perceptual criteria. *J Appl Cryst.* 1992;25:495–503.
- Svergun DI, Koch MHJ. Small-angle scattering studies of biological macromolecules in solution. *Rep Prog Phys.* 2003;66:1735–82. <https://doi.org/10.1088/0034-4885/66/10/R05>
- Svergun DI, Petoukhov MV, Koch MHJ. Determination of domain structure of proteins from X-ray solution scattering. *Biophys J.* 2001;80:2946–53.
- Waterhouse A, Bertoni M, Bienert S, Studer G, Tauriello G, Gumienny R, et al. SWISS-MODEL: homology modelling of protein structures and complexes. *Nucleic Acids Res.* 2018;46:W296–303.
- Yokoyama H, Tsuruta O, Akao N, Fujii S. Crystal structure of *helicobacter pylori* neutrophil-activating protein with a di-nuclear

ferroxidase center in a zinc or cadmium-bound form. *Biochem Biophys Res Commun.* 2012;422:745–50.

SUPPORTING INFORMATION

Additional supporting information can be found online in the Supporting Information section at the end of this article.

How to cite this article: Guerra JPL, Blanchet CE, Vieira BJC, Waerenborgh JC, Jones NC, Hoffmann SV, et al. Controlled modulation of the dynamics of the *Deinococcus grandis* Dps N-terminal tails by divalent metals. *Protein Science.* 2023;32(2):e4567. <https://doi.org/10.1002/pro.4567>